Shape Effect in the Design of Nanowire-Coated Microparticles as Transepithelial Drug Delivery Devices

Vuk Uskoković,[‡,†,*] Kunwoo Lee,[‡,§,†] Phin Peng Lee,[‡] Kathleen E. Fischer,[‡] and Tejal A. Desai[‡,*]

[‡]Therapeutic Micro and Nanotechnology Laboratory, Department of Bioengineering and Therapeutic Sciences, University of California, San Francisco, California 94143, United States, and [§]UC Berkeley/UCSF Graduate Program in Bioengineering, Berkeley, California 94720, United States. [†]These authors have contributed equally to this work.

ABSTRACT While the oral drug delivery route has traditionally been the most popular among patients, it is estimated that 90% of therapeutic compounds possess oral bioavailability limitations. Thus, the development of novel drug carriers for more effective oral delivery of therapeutics is an important goal. Composite particles made by growing nanoscopic silicon wires from the surface of narrowly dispersed, microsized silica beads were previously shown to be able to (a) adhere well onto the epithelium by interdigitating their nanowires with the apical microvilli and (b) increase the permeability of Caco-2 cell monolayers with respect to small organic molecules in direct proportion to their concentration. A comparison between the effects of spherical and planar particle morphologies on the permeability of the epithelial cell layer *in vitro* and *in vivo* presented the subject of this study. Owing to their larger surface area, the planar particles exhibited a higher drug-loading efficiency than their spherical counterparts, while simultaneously increasing the transepithelial permeation of a moderately sized model drug, insulin. The insulin elution profile for planar nanowire-coated particles displayed a continual increase in the cumulative amount of the released drug, approaching a constant release rate for a 1–4 h period of the elution time. An immunohistochemical study confirmed the ability of planar silica particles coated with nanowires to loosen the tight junction of the epithelial cells to a greater extent than the spherical particles did, thus, enabling a more facile transport of the drug across the epithelium. Transepithelial permeability tests conducted for model drugs ranging in size from 0.4 to 150 kDa yielded three categories of molecules depending on their permeation propensities. Insulin belonged to the category of molecules deliverable across the epithelium only with the assistance of nanowire-coated particles. Other groups of drugs, smaller and bigger, respectively, either did not need the carrier to permeate the epithelium or were not able to cross it even with the support from the nanowire-coated particles. Bioavailability of insulin orally administered to rabbits was also found to be increased when delivered in conjunction with the nanowire-coated planar particles.

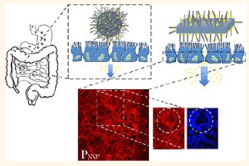

KEYWORDS: Caco-2 · epithelium · insulin · nanowire · oral drug delivery

The ability to control shape, size, and interfacial properties to enhance the functionality of particle-based drug delivery devices is increasingly being recognized.[1] By means of controlling the particle topography, the interfacial energy between the device and the adjacent tissue and the biological response of the latter can be controlled.[2–4] Elongated and asymmetrical particles in particular present a convenient choice for drug delivery devices intended to adhere onto a biological surface.[5,6] Highly irregular, discoid, and cylindroid particles were, for example, shown to adhere to tumor vasculature and be sequestered by the liver, spleen, and lung to a much greater extent than spherical particles did.[7] This shape effect has already been utilized by some biological compounds, including cholesterol platelets and elongated calcium phosphate crystals that comprise atherosclerotic plaque.[8] Namely, their effective adherence onto blood vessel walls is owing to their propensity to form planar particles and thus maximize the surface area in contact with the tissue.[9] A similar strategy can be applied in the design of oral drug delivery carriers whose purpose is to adhere strongly onto the target tissue and resist being carried away by the microflows of the mucous layer.[10]

There are a number of challenges in oral drug delivery,[11–13] including (a) the harsh acidic environment in the gut, (b) rapid clearing of the drug off the epithelial lining, and (c) the finite size limit, ~300 Da,[14] for the paracellular transport of the drug from the intestines and into the bloodstream. In our former studies, we showed that microsized silica beads coated with silicon nanowires present good candidates for adhesive drug delivery devices due to (a) the facility of their loading with drug suspensions *via* the capillary effect,[15] (b) their ability to entwine with and sterically adhere to apical microvilli on the surface of epithelial cells,[16,17] and (c) their ability to increase the tight junction (TJ) permeability and enable a more effective passage for the small molecule drugs across the *in vitro* model of the epithelium.[18] In this study, we modified the shape of the microparticles onto which nanowires are attached from spherical to

* Address correspondence to vuk.uskokovic@ucsf.edu, tejal.desai@ucsf.edu.

Received for review May 4, 2012 and accepted August 18, 2012.

Published online August 18, 2012
10.1021/nn3019865

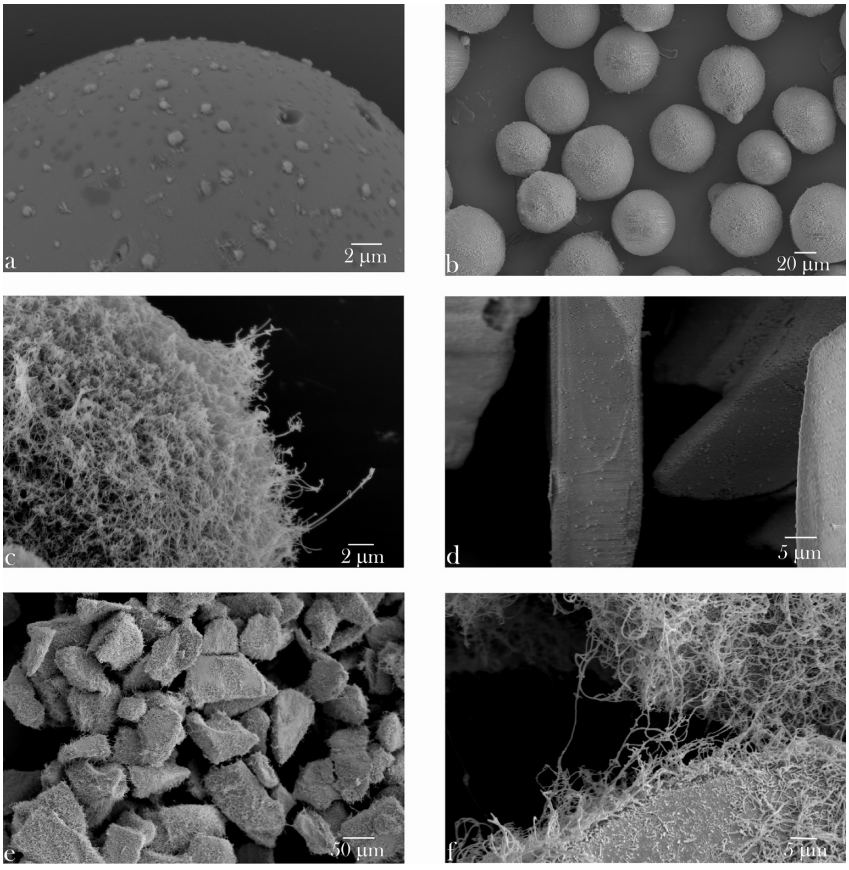

Figure 1. Scanning electron micrographs of spherical microparticles, (a) bare (S_B) and (b, c) coated with nanowires (S_{NW}), and irregularly planar microparticles, (d) bare (P_B) and (e, f) coated with nanowires (P_{NW}), imaged under different magnifications.

planar and analyzed the effects of this microscale morphological variation on the permeability of the epithelium formed *in vitro* by Caco-2, a human colon carcinoma cell line, and *in vivo*.

RESULTS AND DISCUSSION

SEM images of four types of particles utilized in this study are shown in Figure 1: bare spherical (S_B) and planar (P_B) silica microparticles and nanowire-coated spherical (S_{NW}) and planar (P_{NW}) silica microparticles. Spherical particles were narrowly dispersed with a diameter of 30−50 μm. Planar microparticles were less regularly shaped but equally narrowly dispersed, with the average dimensions of 100 × 50 × 5 μm. Aside from their larger surface area in comparison with S particles, they also possessed a more asymmetric, planar geometry, intended to facilitate adhesive interaction with the epithelium. The average length of nanowires grown from the particle surface was 4−8 μm for S_{NW} and 5−10 μm for P_{NW}. For both particles, the diameter of the nanowires was about 60 nm. The diameters of the nanowires are within the endocytic range, but not the lengths too, which prevents them from undergoing endocytosis in the case of detachment from the microparticle surface.

The shape of P particles was rationally designed with a 2-fold purpose (a) to maximize the duration of adhesion to the mucous epithelium of intestines under high shear flow, and (b) to increase the surface area in contact with the epithelium. In the oral delivery platform, the drug permeability and the residence time of the delivery device in intestines are two key factors determining their therapeutic effectiveness. To estimate the adhesion force and resistance to shear, a parallel flow chamber test was conducted and the results have shown a higher average surface retention time for P_{NW} particles *versus* S_{NW} by 20%, with a 60% confidence interval (Figure.2b). The shear pressure of ~70 dyn/cm^2, under which both types of nanowire-coated particles exhibited high retention time, was sufficient to detach most bare P and S particles, confirming that nanowires on the particle surface markedly enhance adhesion. No significant difference in the retention time was observed depending on the initial particle number, suggesting that the percentage of retained particles under the conditions applied herein was independent of the initial number of particles in contact with the cell surface. More importantly, most P_{NW} particles were shown to adhere onto the cell monolayer with their largest faces, further maximizing their surface area in contact with the cells (Figure.2a). Not only did the larger surface area of P particles help them adhere better onto the underlying cell layer, but

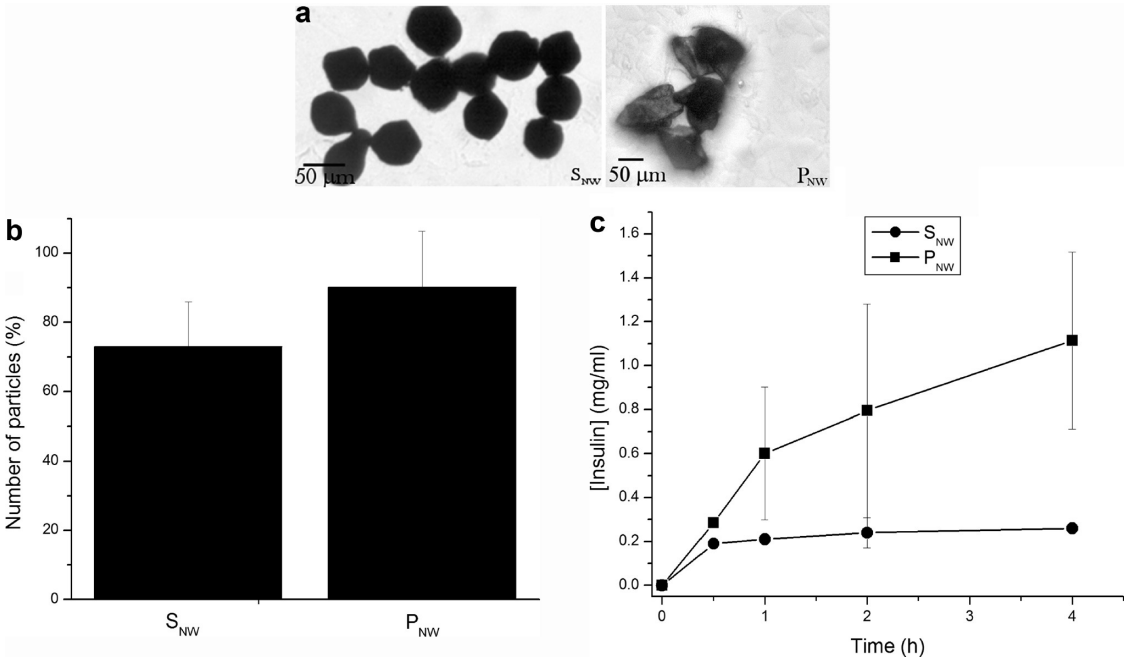

Figure 2. (a) Optical micrographs of S_{NW} and P_{NW} particles under shear flow; (b) percentage of nanowired-coated microparticles retained on the Caco-2 cell monolayers following the application of 70 dyn/cm^2 of shear flow; (c) temporal concentration profile for the elution of insulin from different microparticles.

their lesser surface area facing the flow additionally explains for their ability to stay longer in contact with the underlying cell layer when subjected to shear flow.

Because a major goal of drug delivery is to maintain the drug levels within the therapeutic window with a minimal dosage, the drug loading capacity is a primary criterion determining the therapeutic effectiveness of a device. Therefore, we tested different shapes of microparticles, P_{NW} and S_{NW}, for their ability to capture insulin and elute it in 4 h. This time scale was chosen because previous studies have shown that S_{NW} do not remain in the small intestine for longer than 3 h.[17] Figure 2c shows the drug elution profile of insulin-loaded microparticles, S_{NW} and P_{NW}. Spherical particles displayed no significant concentration changes as a function of elution time, while P_{NW} ones demonstrated a continuous increase of insulin concentration in the supernatant in direct proportion to the incubation time, approaching a constant release rate for 1−4 h time period. P_{NW} demonstrated approximately 5 times higher insulin loading capacity than S_{NW}. Geometric calculations based on the results of the morphological analysis of S and P particles (Figure 1) showed that the surface area of P particles is 3−3.5 times higher than that of S ones in the samples of identical weight, explaining why the loading efficiency was higher for P_{NW} particles than for S_{NW} ones. As expected, P_{NW} particles adsorbed more insulin than P_B due to (a) the additional surface area created by nanowires, and (b) the capillary effect by which they are able to effectively capture drug molecules in spite of the unfavorable concentration gradients. Conversely, the network of intertwined nanowires is responsible for the gradual increase in the cumulative amount of the eluted drug in the case of P_{NW} particles. As estimated from the comparison with the insulin release from P_B particles (data not shown), P_{NW} particles contained almost 70% of insulin stored in reservoirs between nanowires on their surface. The gradual release of the drug is expected to be a favorable factor for oral delivery devices because an early burst of the released drug may lower the therapeutic efficacy of the carrier.

Augmenting the transepithelial delivery efficiency without compromising the selective permeability of the epithelium is one of the biggest challenges faced by oral drug delivery. The permeability tests were conducted in order to measure the amount of insulin delivered across Caco-2 cell monolayers. As shown in Figure 3a,b, all spherical particles induced lower levels of permeability in comparison to P_{NW}, irrespective of whether the drug was loaded onto the particles prior to the test (Figure 3a) or added separately to the apical compartments (Figure 3b). P_{NW} has led to the highest concentration of basolateral insulin and, when particles loaded with insulin were applied, a drug delivery profile typified by a gradually increasing cumulative concentration of the released drug for the first 2 h of incubation was obtained. The similarity of the temporal trend for the given transepithelial delivery to the insulin elution graph shown in Figure 2c unequivocally suggests the kinetic contingency of the drug permeability to the drug release, especially because such an increasing trend in basolateral concentration of insulin was absent when the drug and the particles were

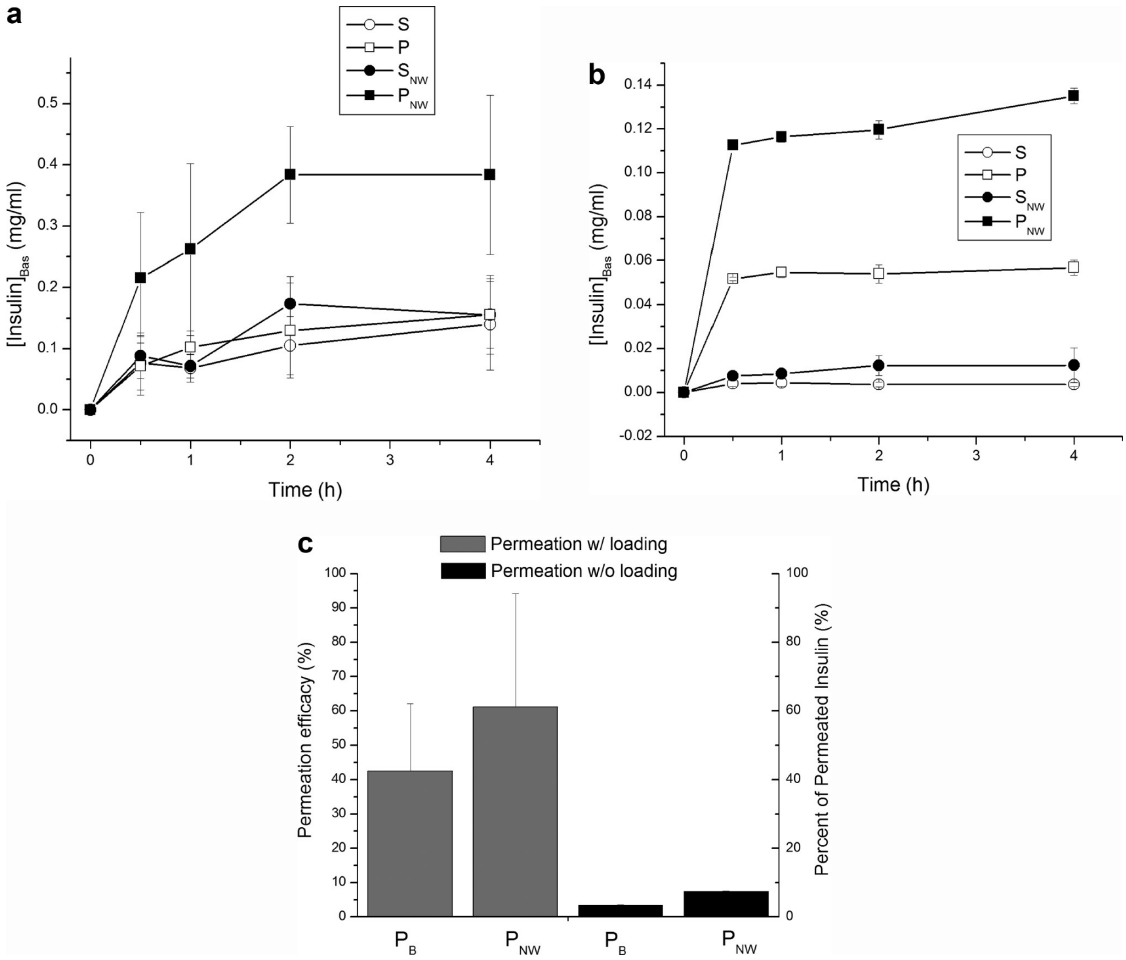

Figure 3. (a) Concentration of insulin permeated across the Caco-2 cell layer membrane upon the application of different particles loaded with insulin: S_B, S_{NW}, P_B, and P_{NW}; (b) concentration of insulin permeated across the Caco-2 cell layer membrane when the particles and insulin were added separately to the apical compartments; (c) permeation efficacy using insulin-loaded P_{NW} particles and the percentage of permeated insulin when P_{NW} particles and insulin were added separately, after 30 min incubation. Permeation efficacy was calculated as a ratio between the eluted amount of the drug and the permated amount of the drug. Data are shown as averages with error bars representing standard deviation (*$p < 0.005$ with respect to the control group). The statistical difference between the permeation efficacy of P_B and P_{NW} with loading has the two-tailed *P* value equal to 0.44; by conventional criteria, this difference is considered to be not statistically significant.

added separately (Figure 3b). Geometric calculations have shown that the surface area of P particles in contact with the cell monolayer is approximately 10 times higher than for S particles in samples of identical weight, which explains for their greater efficiency in promoting the transepithelial delivery of insulin. In contrast, the fact that P_B particles did not deliver insulin across the cell layer as effectively as P_{NW} supports the hypothesis that the nanostructured topography present on the microparticle surface is a key influence on transepithelial drug delivery process.

Drug permeation across the epithelium is in this case expected to be influenced by two factors: (a) drug elution and (b) particle geometry. The purpose of the drug permeability test without prior drug loading was to kinetically decouple the drug release effect from particle geometry and nanostructured topography. When the permeability test was conducted by separately adding insulin and microparticles apically, both P particles, P_B and P_{NW}, induced higher permeability than any of the S ones (Figure 3b). Despite the similarity in the drug permeation trend between the two methods, the percentage of the drug delivered across the epithelium was significantly higher when insulin-loaded P_{NW} particles were applied (Figure 3c). Even though the amount of free drug in the apical compartment was lower when particles loaded with the drug were used, the resulting permeability was higher than in the case when the particles and the drug were added separately. These results signify that the presence of the drug in the immediate vicinity of the nanowire-induced disruption of the epithelium is vital to ensure a facile delivery process. Because the concentration of insulin is highest in the close proximity of the particle and gradually decreases as one approaches the bulk medium, diffusion effects will favor the drug transport directly off the particle surface if the nanowires manage to widen the tight junction spacing. Loading of the

drug onto the particles also prevents the unfavorable blocking effect, whereby the nanowires, by virtue of their proximity to the epithelium surface during their interaction with the cell monolayer, competes spatially with the diffusion of the drug from the bulk medium. Lying flat on the cell monolayer surface, a P_{NW} particle with its large surface can be visualized to impede the bulk diffusion of the drug across the underlying epithelium, an effect that could be circumvented by releasing the drug directly off the particle surface in contact with the epithelium.

The conclusion can be drawn that the shape of microparticles influences the permeability of insulin across Caco-2 cell monolayers. Both the surface area in contact with the epithelium and the actual nanotopography are presumed to affect the mechanotransduction pathways that allow for an effective transepithelial transport of the drug. The role of nanowires in enhancing permeation could be accomplished by their perforation of the intercellular spacing and thereby extension of the space available for transepithelial diffusion. A more plausible explanation could be that the nanostructures in contact with the epithelium prompt the cells to reach up to them, thereby widening the intercellular spacing. Increased permeability of small molecules across the epithelium induced by S_{NW} particles was reported previously.[18] For P particles, the surface nanowires induced a 2-fold increase in permeability *versus* nanowire-free particles, an effect that is more pronounced than the previously reported one. The augmented effect of P_{NW} particles in comparison with S_{NW} can be explained by the larger surface area of interaction between the nanowires and the epithelium.

To examine the effects of P_{NW} particles on the integrity of the tight junction, an intercellular protein complex that regulates the paracellular transport of molecules across the epithelium,[19−21] a morphological comparison between cell monolayers treated with S_{NW} and P_{NW} was conducted after the 4 h delivery. As shown in Figure 4a,b, P_{NW} particles showed a clear tendency to ruffle the ZO-1 pattern, indicating a mildly disruptive effect on the tight junction, through which a higher rate of drug delivery across the epithelium is enabled. Approximately 60−70% of the ZO-1 pattern lined up along the tight junction was ruffled upon the application of 5 mg of NW particles per cm^2, as opposed to only 8% in the control sample and 10% in the sample incubated with an equal amount of S_{NW} microbeads. Such a jagged profile of a junctional protein, along with occasionally seen double lines, is an indicator of a structurally disrupted, but not dysfunctional, epithelial membrane.[22,23] A comparison of the fluorescence intensity of the ZO-1 pattern normalized to the surface area yielded significantly lower intensity for ZO-1 of cells incubated with P_{NW} than for that incubated with S_{NW} or the negative control (Figure 4c). Because the paracellular permeability is thought to be inversely proportional to the density of tight junctional strands,[24−26] the detected decrease in the density of the perijunctional ZO-1 molecules is directly indicative of an increased paracellular permeability of Caco-2 cell monolayers in contact with P_{NW} particles. Another observation consistent with the loosening of the tight junction that P_{NW} particles induced to a markedly greater extent than S_{NW} has come from the comparison of the width of the ZO-1 pattern. As also shown in Figure 4c, in the presence of P_{NW} particles, it is twice lower with respect to both the negative control and the cells treated with S_{NW} particles. Once sufficient surface coverage of the cell monolayer by P_{NW} particles is achieved, any further addition of particles, mainly forming stacked-up agglomerates, does not contribute to a further decrease in the tight junction width (Figure 4d). These results also confirm that TJ loosening is more likely to be caused by nanostructures than by the weight effect of microparticles on the underlying epithelium. Concordantly, immunofluorescent staining of claudin-1, the results of which are shown in Figure 5, demonstrates a greater degree of diffuseness of the transmembrane protein following incubation with P_{NW} particles in comparison with the S_{NW} ones, an effect known to coincide with the application of chemical agents that increase the paracellular permeability of Caco-2 cells.[27,28] Namely, as the spacing between tightly packed and polarized epithelial cells increases, the transmembrane proteins become partially endocytosed and withdrawn toward the cytoplasmic environment, contributing to this diffusion effect and less distinct cell boundary outlines.

Although we demonstrated that the physical contact between nanowire-coated microparticles and the epithelium can facilitate the transepithelial transport of drugs, the question remained how big the drug molecule has to be before this transport becomes unfeasible. To shed light on a possible answer, we conducted a series of permeability tests on different molecular weights of FITC-conjugated molecules, ranging from the smallest, FITC *per se* (389 Da), to the largest, FITC-IgG (150 kDa), without a prior drug loading. The results of the comparative effect of P_{NW} particles on the permeability of differently sized model drugs across Caco-2 cell monolayer are summed in Figure 6. Three different groups of drug molecules could be outlined depending on their sizes and the corresponding permeation profiles. Molecules from the first group, including 332 Da fluorescein and its derivative FITC, readily cross the epithelium, even without nanowires facilitating the delivery process. Despite their propensity to cross the epithelium, simultaneous subjugation of the latter to interaction with nanowires accelerated the permeation process, presumably as the result of reorganization of the tight junction in the direction of its increased permeability to small molecules. Insulin

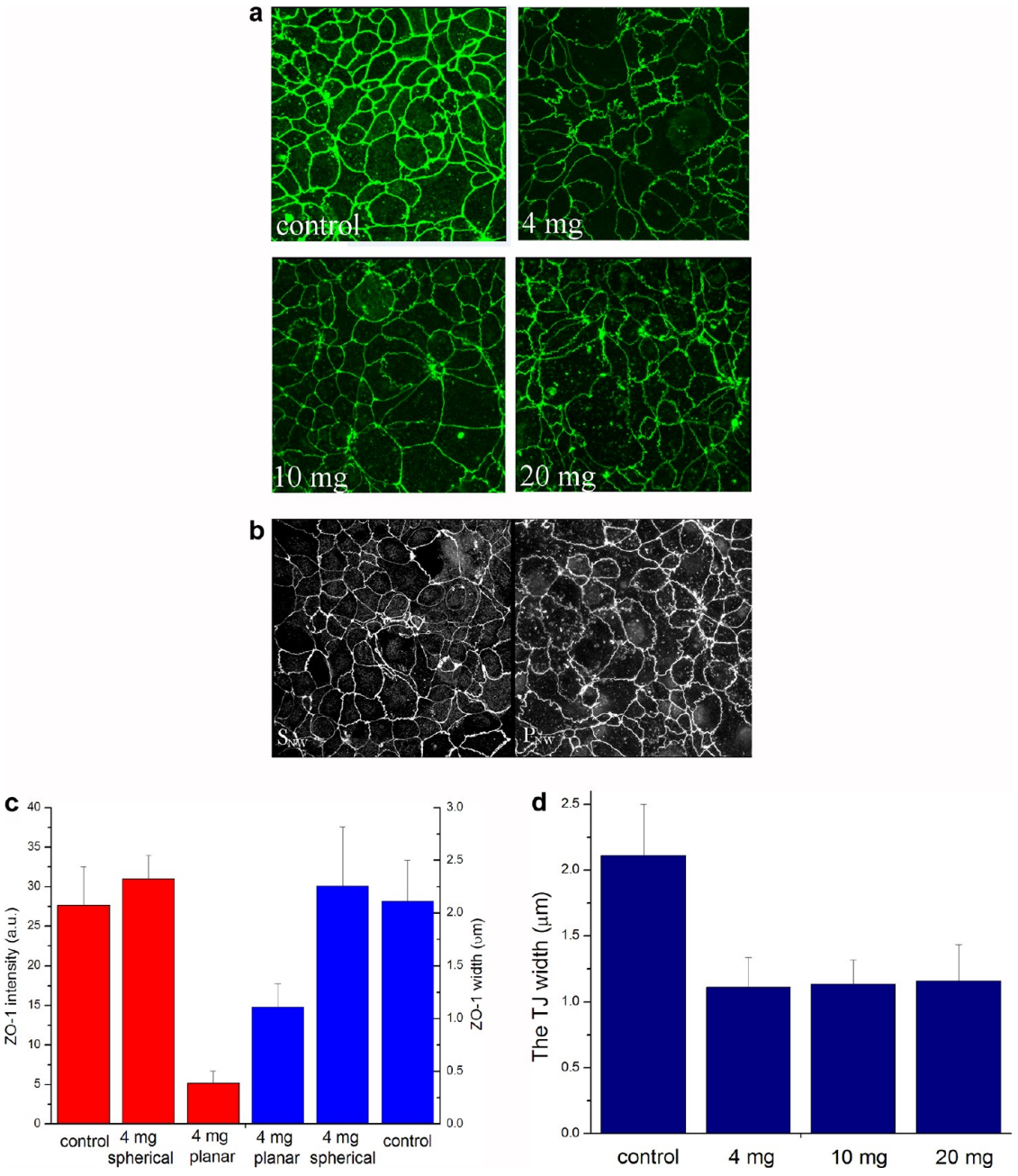

Figure 4. (a) Fluorescent staining of ZO-1 molecules in Caco-2 cell monolayers treated for 4 h with no particles (control) and with different amounts of P_{NW} particles per cm^2, imaged under identical excitations; (b) a comparison between the fluorescently stained ZO-1 pattern of Caco-2 cell monolayers treated for 4 h with P_{NW} and S_{NW} particles; (c) a comparison between the average pixel intensity of ZO-1-tagged fluorescent IgG and the width of ZO-1 conglomerates at the tight junction for Caco-2 cells incubated without any particles (control) and in the presence of 4 mg/cm^2 of S_{NW} and P_{NW} particles; (d) a comparison between the width of ZO-1 conglomerates at the tight junction for Caco-2 cells incubated without any particles (control) and in the presence of different amounts of P_{NW} particles cm^2. Data are shown as averages with error bars representing standard deviation (*$p < 0.005$ with respect to the control group). All images were taken at 100× magnification in oil. The size of each micrograph is 750 × 750 μm.

(5.6 kDa) and 4 kDa FITC-dextran belong to the second group of molecules, which could be delivered across the epithelium only with the assistance of microparticles. The third group includes even bigger molecules, from 10 kDa FITC-dextran to 150 kDa FITC-IgG, which cannot be transported across the epithelium even with assistance of the microparticles. In the case of FITC-IgG, not only did the increased amounts of either P_{NW} or S_{NW} particles fail to induce higher permeability, but the microparticles also blocked the paths for the natural, transcellular cell uptake of the drug. These are important considerations as we advance to an *in vivo* model.

Bioavailability of orally administered insulin is exceptionally low *in vivo*, with less than 0.1% of the oral dose reaching the bloodstream.[29] Recent advances in polymeric delivery have brought bioavailability of oral

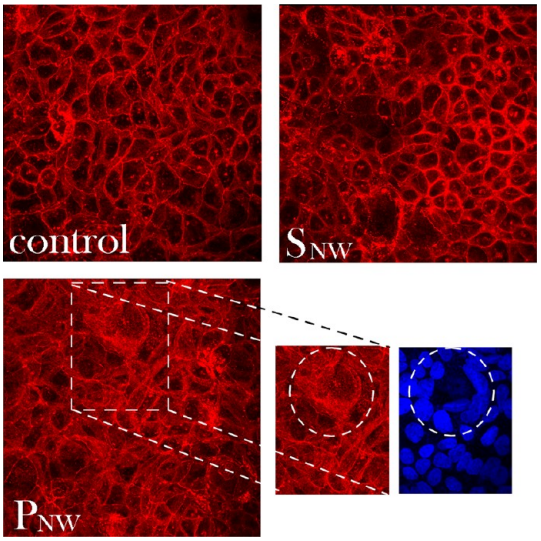

Figure 5. Immunofluorescent staining of claudin-1 molecules (red) and cell nucleus (blue) in Caco-2 cell monolayers treated for 4 h with either no particles (control) or with 2 mg/cm^2 of S_{NW}/P_{NW} particles. All images were taken at 60× magnification in oil. The size of each image is 450 × 450 μm. The magnified part of the P_{NW} image shows an area of the epithelium around a P_{NW} particle, typified by a diffuse claudin-1 pattern and no distinct tight junction.

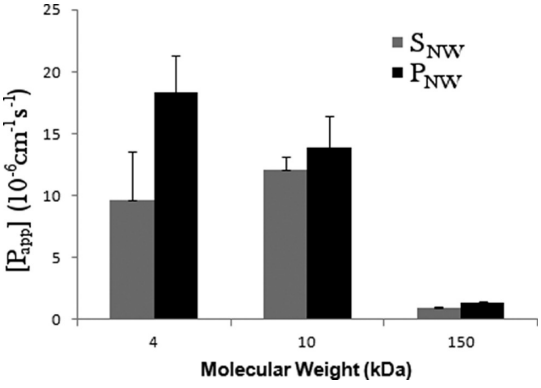

Figure 6. Comparison between the apical-to-basolateral permeability of Caco-2 cell monolayer for differently sized drug molecules in the presence of S_{NW} and P_{NW} particles. Data are shown as averages with error bars representing standard deviation (*p < 0.005 with respect to the control group). The statistical difference between the permeability coefficients of S_{NW} and P_{NW} at 10 kDa has the two-tailed P value equal to 0.4; by conventional criteria, this difference is considered to be not statistically significant.

insulin into the range of 5 – 15,[30] suggesting that suitable carriers present a viable pharmaceutical choice for oral delivery of insulin. Here, we show a baseline oral bioavailability of 4.9 over the 2 h of testing, as compared to 5.9 with S_{NW} delivery and 6.7 with P_{NW} delivery (Figure 7). P_{NW} delivery exhibited maximal blood concentrations at 1 h, whereas S_{NW} showed maximal concentrations at 2 h. At time points that extended beyond the 2 h, endogenous insulin levels became higher that the delivered insulin levels, as in agreement with previously performed oral insulin

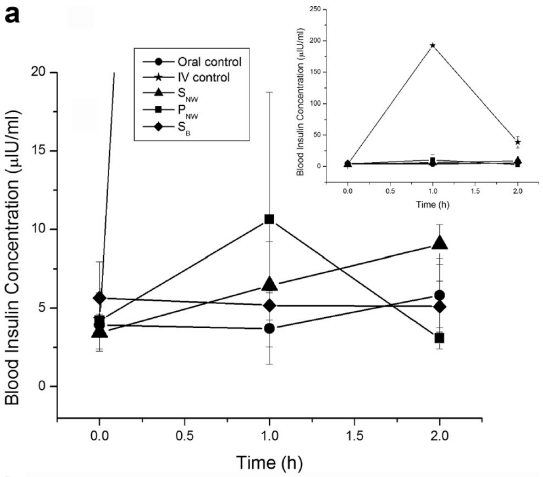

b

Group	F	AUC (uIU*hr/ml)	CL (ml/hr)	K_e (1/hr)	$t_{½}$ (hours)
S_B	4.01%	8.58	5.12	0.0162	42.62
S_{NW}	5.93%	12.69	3.46	0.0109	63.04
P_{NW}	6.67%	14.28	3.07	0.0097	70.94
IV	n/a	214.13	0.20	0.0006	1063.65
Oral	4.94%	10.57	4.15	0.0131	52.52

Figure 7. Pharmacokinetic properties of drug delivery devices in rabbits. (a) Blood insulin concentration after dosing of 9.8 IU/kg. Error bars indicate standard deviation with a sample size of four animals per group. Inset shows plot with a full range of IV control; b) Pharmacokinetic constants calculated for each experimental group. F, bioavailability, AUC, area under the curve; CL, clearance; K_e, elimination rate; $t_{1/2}$, half-life.

delivery tests on rabbits.[31] Still, both S_{NW} and P_{NW} showed a longer half-life than the oral control, with greater AUC and lower clearance. The oral controls were significantly different from the IV control at 1 and 2 h and from S_{NW} at 2 h (p < 0.05). Thus, the use of S_{NW} and P_{NW} compares favorably *in vivo* with other delivery devices, despite the minimal optimization of nanowire coating or the loading technique. The fact that the oral delivery by means of S_{NW} led to the highest concentrations of insulin in blood 2 h following the administration among all the drug carriers tested can be explained by the considerably more variable geometry of the gastrointestinal tract compared to the flow chamber where the adhesion tests were carried out. It is possible that the microscopically observed clustering of P_{NW} particles allowed them to pass through the digestive tract more easily, in contrast with S_{NW} particles whose convex surfaces may have made them prone to become lodged in the network of villi and the rugae in the intestine.

CONCLUSION

By means of controlling the shape of the particles, their contact surface could be tailored for the given purpose. For particles meant to have a high retention time in the bloodstream, spherical morphologies, having the lowest contact surface, would present the natural choice. In contrast, when viable adherence of

the drug delivery agents in spite of the mucous layer lining the epithelium is sought, elongated or irregularly shaped particles would perform better in theory. Shape and texture of the particles can thus be optimized to promote adhesion by means of simple steric effects. In this work, we have shown that irregularly planar silica particles coated with silicon nanowires exhibited a higher drug loading capacity than their spherical counterparts owing to their three times larger surface area per unit weight. Simultaneously, as a result of a larger surface area in contact with the cell layer, the planar particles increased the transepithelial permeation of a moderately sized model drug, insulin. Transepithelial permeability tests were conducted for a number of model drug molecules, ranging from fluorescein isothiocyanate to 4−10 kDa sized dextrans to bovine serum albumin to immunoglobulin G, and three categories of molecules were established based on their sizes and the corresponding permeation propensities. Insulin was found to belong to the second category of molecules, which could be delivered across the epithelium only with the assistance of nanowire-coated particles. Categories below and above belonged to smaller and bigger drugs, respectively, that either needed not the carrier to permeate the epithelium or were not able to cross it even with the support from the nanowire-coated particles, spherical or planar. Bioavailability of insulin orally administered to rabbits was also found to be increased when delivered in conjunction with the nanowire-coated particles. Lastly, by demonstrating that the effects of nanotopography can be scaled by increasing the surface area of interaction, we have opened the doors to the creative use of geometry in future devices aiming to incorporate this technology for various biomedical applications.

METHODS

Spherical and Planar Silica Microparticles Coated with Nanowires. Spherical (S) and planar (P) silica microparticles were provided by Nanosys, Inc., in two forms: bare (S_B, P_B) and coated with silicon nanowires (S_{NW}, P_{NW}). The particles were synthesized by means of chemical vapor deposition of silicon ions onto silica microparticles sputtered with gold.[32] Scanning electron microscopy (SEM, Hitachi, S-4300SE/N) was used for the morphological and size analysis of the four types of particles utilized in this study. The average dimensions of particles were determined from an SEM analysis and used to calculate the surface area of an averagely sized particle of a given type.

Caco-2 Cell Culture. The human intestinal Caco-2 cells were obtained from American Tissue Culture Collection (ATCC, Rockville, MD) and cultured in Eagle's Minimum Essential Medium with Earle's balanced salt solution, 1 mM sodium pyruvate, 20% fetal bovine serum (Sigma), and 1% penicillin−streptomycin antibiotic solution. In all experiments, the cells were seeded in 24-well plates at a density of 7.5×10^4 cells per well either on glass coverslips (Fisherbrand) or in the apical compartments of TranswellsTM. Seeded at the given cell density, the cells would reach confluency in 5−7 days. Every 7 days, the cells were detached from stock cultures by means of trypsin (0.25 wt %) digestion, washed, centrifuged (1000 rpm × 3 min), resuspended in 10 mL of media, and subcultured in 1:7 volume ratio. The cultures were regularly examined under an optical microscope to monitor their growth and possible contamination. Cell passages 22−35 were used for the hereby reported experiments. Caco-2 cell line, originally established in 1977,[33] has been a standard model system for assessing intestinal epithelial permeability.[34] It has also been proven as a viable model for the *in vitro* investigation of various drug delivery vehicles.[35−37] However, numerous problems were also associated with the usage of this cell line as an *in vitro* model of the epithelium, including the following:[38−41] (a) variability in the cell behavior depending on the cell clone, passage, and culturing conditions; (b) cell aggregation loci may lead to erroneously estimated drug permeability; (c) the transepithelial transport efficacy is sensitive to the nature of the buffers and the solid surface onto which the cells adhere; (d) assumed linearity of the drug transport process implicit in the concept of permeability coefficient. To minimize the effects of these and other artifacts, the results of all the experiments were compared with the simultaneously cultured controls subjected to no particle/drug treatments.

Shear Flow Measurements. The adhesion of the particles onto Caco-2 cell monolayers under shear flow was measured using a parallel plate flow chamber (Glycotech, Gaithersburg, MD). The particles were allowed to adhere onto the cell monolayer for 5 min prior to assembly of the chamber. The cell culture media flow rate was increased to produce the shear pressure of ~70 dyn/cm^2. Images of adhering particles at different time points were taken on an Olympus BX60 microscope using NIS-Elements Advanced Research software. Their surface retention coefficients were estimated by comparing the cell count per image captured under 10× magnification (a) immediately after the assembly of the chamber and subjection of the particles to the shear flow and (b) 5 min later. The number of particles captured per image ranged between 20 and 100. ImageJ software was used for subsequent particle number counting.

Drug Loading and Elution. Solvent-evaporation-induced capillary effect was used as a mechanism for loading the particles with the moderately sized model drug, insulin. A total of 2 mg of microparticles were immersed in 166 μL of the loading solution and heated at 35 °C for approximately 24 h (until dry). The loading solution comprised 10 mg/mL of bovine pancreatic insulin (Sigma) dissolved in phosphate buffer saline (PBS). To remove the residual, unloaded drug, washing with PBS was carried out, after which the particles were transferred to a new vial and weighed. Particles loaded with insulin were suspended in 0.5 mL of PBS and kept on a shaker plate for 4 h. A portion of the supernatant (25 μL) was periodically extracted to quantify the amount of eluted insulin. The quantification was performed using a regular bicinchoninic acid (BCA) protein assay. The absorbance of the samples was read at λ = 562 nm following the manufacturer's guidelines.

Drug Permeability across Caco-2 Cell Monolayers. Confluent Caco-2 cells seeded in high-density 0.3 cm^2 cell culture inserts with 0.4 μm pore size (Falcon) placed in 24-well plates were exposed apically to 1−20 mg of particles (S_B, P_B, S_{NW}, P_{NW}) in 500 μL of the phenol-free cell culture media. The basolateral compartments initially contained 1 mL of PBS. Separate permeability experiments were carried out (a) with insulin-loaded microparticles and (b) with microparticles and separately added 1 mg/mL solutions of drugs of various sizes: 389 Da fluorescein isothiocyanate (FITC), 4 kDa FITC-dextran, 5.6 kDa insulin, 10 kDa FITC-dextran, 66 kDa FITC-BSA, and 150 kDa FITC-IgG. FITC was applied as a sodium salt and thus permeated the cell layers in ionized form. A portion of the supernatant (25 μL) was periodically extracted from the basolateral compartment to quantify the amount of eluted drug using either BCA assay or a Packard Fluorocount fluorometer at the excitation λ = 495 nm and the emission λ = 518 nm. To mimic the physiological conditions in the intestines, the 4 h incubations were performed by keeping the inserts on a shaker plate (120 rpm). All the experiments were done in triplicate and each experimental replica was analyzed

for the drug content also in triplicate ($n = 3 \times 3$). Prior to the start of the experiment, an increase in the cell density was monitored by means of daily TEER measurements. TEER values higher than 300 $\Omega \cdot cm^2$ were taken as a sign of confluent cell monolayers. To ensure that the cells are furthermore polarized, with the appropriate tight junctions, TEER was allowed to increase through the next 48 h or so. The initial TEER at the onset of the permeability experiments was between 600 and 1000 $\Omega \cdot cm^2$, matching the earlier reported range of values for polarized monolayers of confluent Caco-2 cells and the epithelial lining of the colon.[42,43] The permeability coefficients (P_{app}) for different fluorescent drugs were calculated using the following equation,[44] in which dq/dt is the rate of change in the amount of fluorescence on the basolateral side converted to fluorophore concentration units (mg/mL), A is the surface area of the inserts, and $C°$ is the initial concentration of fluorophore applied in the apical compartment (mg/mL):

$$P_{app} = \frac{dq}{dt} \times \frac{1}{A \times C°} \quad (1)$$

Immunofluorescence for Zonula Occludens-1 (ZO-1) and Claudin-1. Upon reaching full confluency, Caco-2 cells in 24-well plates were treated with different amounts of S_{NW} and P_{NW} particles (4, 10, or 20 mg per well) suspended in 500 μL of the cell culture media and incubated for 4 h at 37 °C. The media along with the particles were then aspirated and the cells were washed with PBS and fixed for either 5 min in −20 °C methanol in the case of staining of ZO-1 or 15 min in 3.7 wt % paraformaldehyde at room temperature in the case of staining of claudin-1. The cells were then washed three times with PBS, 5 min each, and then with the blocking solution (PBT = 1% BSA, 0.1% Triton X-100 in PBS) two times, 5 min each. The cells were then blocked and permeabilized in PBT for 1 h and incubated with 200 μL/well primary antibody, 10 μg/mL rabbit anti-ZO-1 (Zymed Lab), or 10 μg/mL rabbit anticlaudin-1 (Abcam) in PBT overnight at 4 °C. After the overnight incubation, the cells were washed with PBS 3×10 min and then incubated with 150 μL/well secondary antibody, 2.5 μg/mL AlexaFluor 555 goat antirabbit IgG (Invitrogen), and 20 μg/mL 4′,6-diamidino-2-phenylindole dihydrochloride nuclear counterstain (DAPI, Invitrogen), all in PBT for 1 h at room temperature. After washing with PBS 3×5 min, the coverslips containing the fixed and stained cells were mounted onto glass slides using Vectashield and nail hardener and imaged in oil under a confocal laser scanning microscope, C1si (UCSF Nikon Imaging Center) at 60−100× magnification. All the experiments were done in triplicates and the staining immunofluorescence pixel intensity was measured from four randomly selected images in each sample ($n = 4 \times 3$). Volume-rendered z-stack images (12−15 of them) spaced by 1 μm were collected at identical laser intensities and analyzed for the fluorescence intensity, the thickness of ZO-1 conglomerates and the percentage of the ruffled TJ pattern using ImageJ and NIS Elements software. As a part of this semiquantitative analysis, the thickness of ZO-1 conglomerates at the tight junction was measured as half-width of peaks obtained by plotting the fluorescence intensity profiles across the cell boundary.

***In Vivo* Dosing and Pharmacokinetics.** New Zealand white rabbits were orally dosed with 50 mg of insulin-loaded particles in a #4 gelatin capsule. Experimental groups were insulin-loaded S_B ($n = 4$), insulin-loaded S_{NW} ($n = 4$), insulin-loaded P_{NW} ($n = 4$), an intravenous (IV) administration control ($n = 4$), and an oral administration control (*via* oral gavage, $n = 3$). Controls were orally or intravenously dosed with 2 mg of insulin dissolved in PBS, or 9.8 IU/kg, the amount expected to be released from 50 mg loaded S_{NW}. Blood samples were taken before dosing and at 1 and 2 h, and assayed for insulin *via* ELISA. Absolute bioavailability (F_{abs}) was calculated as a ratio between the areas under the blood plasma drug concentration *versus* time curves (AUCs) for dosages administered orally and by IV means.

Conflict of Interest: The authors declare no competing financial interest.

Supporting Information Available: Results of an MTT *in vitro* toxicological assay, demonstrating no significant decrease in the viability of Caco-2 cells incubated with any of the particles analyzed in this study (S, P, S_{NW}, and P_{NW}). This material is available free of charge *via* the Internet at http://pubs.acs.org.

Acknowledgment. Confocal microscopy data for this study were acquired at the Nikon Imaging Center at UCSF. This research was conducted with funding from the NIH Grant EB01166401. We thank Nanosys, Inc. for fabrication of the nanowire particles.

REFERENCES AND NOTES

1. Tao, S. L.; Desai, T. A. Microfabricated Drug Delivery Systems: from Particles to Pores. *Adv. Drug Delivery Rev.* **2003**, *55*, 315–328.
2. Thakar, R. G.; Chown, M. G.; Patel, A.; Peng, L.; Kumar, S.; Desai, T. A. Contractility-Dependent Modulation of Cell Proliferation and Adhesion by Microscale Topographical Cues. *Small* **2008**, *4*, 1416–1424.
3. Motlagh, D.; Senyo, S. E.; Desai, T. A.; Russell, B. Microtextured Substrata Alter Gene Expression, Protein Localization and the Shape of Cardiac Myocytes. *Biomaterials* **2003**, *24*, 2463–2476.
4. Ainslie, K. M.; Tao, S. L.; Popat, K. C.; Desai, T. A. *In Vitro* Immunogenicity of Silicon-Based Micro- and Nanostructured Surfaces. *ACS Nano* **2008**, *2*, 1076–1084.
5. Decuzzi, P.; Pasqualini, R.; Arap, W.; Ferrari, M. Intravascular Delivery of Particulate Systems: Does Geometry Really Matter? *Pharm. Res.* **2009**, *26*, 235–243.
6. Lee, S. Y.; Ferrari, M.; Decuzzi, P. Design of Bio-Mimetic Particles with Enhanced Vascular Interaction. *J. Biomech.* **2009**, *42*, 1885–1890.
7. van de Ven, A. L.; Kim, P.; Haley, O.; Fakhoury, J. R.; Adriani, G.; Schmulen, J.; Moloney, P.; Hussain, F.; Ferrari, M.; Liu, X.; et al. Rapid Tumoritropic Accumulation of Systemically Injected Plateloid Particles and Their Biodistribution. *J. Controlled Release* **2012**, *158*, 148–155.
8. Uskoković, V. Insights into Morphological Nature of Precipitation of Cholesterol. *Steroids* **2008**, *73*, 356–369.
9. Uskoković, V. Composites Comprising Cholesterol and Carboxymethyl Cellulose. *Colloids Surf., B* **2008**, *61*, 250–261.
10. Tao, S. L.; Desai, T. A. Gastrointestinal Patch Systems for Oral Drug Delivery. *Drug Discovery Today* **2005**, *10*, 909–915.
11. Fasinu, P.; Pillay, V.; Ndesendo, V. M.; du Toit, L. C.; Choonara, Y. E. Diverse Approaches for the Enhancement of Oral Drug Bioavailability. *Biopharm. Drug Dispos.* **2011**, *32*, 185–209.
12. Soares, A. F.; Carcalho Rde, A.; Veiga, F. Oral Administration of Peptides and Proteins: Nanoparticles and Cyclodextrins as Biocompatible Delivery Systems. *Nanomedicine* **2007**, *2*, 183–202.
13. Basit, A. W. Advances in Colonic Drug Delivery. *Drugs* **2005**, *65*, 1991–2007.
14. Dowty, M. E.; Messing, D. M.; Lai, Y.; Kirkovsky, L. ADME. In *ADMET for Medicinal Chemists: A Practical Guide*; Tsaioun, K., Kates, S. A., Eds.; John Wiley & Sons: Hoboken, NJ, 2011; p 151.
15. Fischer, K. E.; Jayagopal, A.; Nagaraj, G.; Daniels, R.; Li, E.; Silvestrini, M.; Desai, T. A. Nanoengineered Surfaces Enhance Drug Loading and Adhesion. *Nano Lett.* **2011**, *11*, 1076–1081.
16. Fischer, K. E.; Nagaraj, G.; Daniels, R. H.; Li, E.; Cowles, V. E.; Miller, J. L.; Bunger, M.; Desai, T. A. Hierarchical Nanoengineered Surfaces for Enchanced Cytoadhesion and Drug Delivery. *Biomaterials* **2011**, *32*, 3499–3506.
17. Fischer, K. E.; Aleman, B. J.; Tao, S. L.; Daniels, R. H.; Li, E. M.; Bunger, M. D.; Nagaraj, G.; Singh, P.; Zettl, A.; Desai, T. A. Biomimetic Nanowire Coatings for Next Generation Adhesive Drug Delivery Systems. *Nano Lett.* **2009**, *9*, 716–720.
18. Uskoković, V.; Lee, P. P.; Walsh, L.; Fischer, K. E.; Desai, T. A. The Effect of PEGylation on Particle-Epithelium Interactions. *Biomaterials* **2012**, *33*, 1663–1672.
19. Takahashi, A.; Kondoh, M.; Kodaka, M.; Yaqi, K. Peptides as Tight Junction Modulators. *Curr. Pharm. Des.* **2011**, *17*, 2699–2703.

20. Yeh, T. H.; Hsu, L. W.; Tseng, M. T.; Lee, P. L.; Sonjae, K.; Ho, Y. C.; Sung, H. W. Mechanism and Consequence of Chitosan-Mediated Reversible Epithelial Tight Junction Opening. *Biomaterials* **2011**, *32*, 6164–617.
21. Johnson, P. H.; Frank, D.; Constantino, H. R. Discovery of Tight Junction Modulators: Significance for Drug Development and Delivery. *Drug Discovery Today* **2008**, *13*, 261–267.
22. Moyes, Sz. M.; Morris, J. F.; Carr, K. E. Macrophages Increase Microparticle Uptake by Enterocyte-Like Caco-2 Cell Monolayers. *J. Anat.* **2010**, *217*, 740–754.
23. Liu, M.; Yang, X.; Fan, J.; Zhang, R.; Wu, J.; Zeng, Y.; Nie, J.; Yu, X. Altered Tight Junctions and Fence Function in NRK-52E Cells Induced by Aristolochic Acid. *Hum. Exp. Toxicol.* **2012**, *31*, 32–41.
24. Claude, P. Morphological Factors Influencing Transepithelial Permeability: A Model for the Resistance of the Zonula Occludens. *J. Membr. Biol.* **1978**, *39*, 219–232.
25. Marcial, M. A.; Carlson, S. L.; Madara, J. L. Partitioning of Paracellular Conductance Along the Ileal Crypt-Villus Axis: A Hypothesis based on Structural Analysis with Detailed Consideration of Tight Junction-Structure Function Relationships. *J. Membr. Biol.* **1987**, *80*, 59–70.
26. Shen, L.; Weber, C. R.; Raleigh, D. R.; Yu, D.; Turner, J. R. Tight Junction Pore and Leak Pathways: A Dynamic Duo. *Annu. Rev. Physiol.* **2011**, *73*, 283–309.
27. Sander, G. R.; Cummins, A. G.; Powell, B. C. Rapid Disruption of Intestinal Barrier Function by Gliadin Involves Altered Expression of Apical Junctional Proteins. *FEBS Lett.* **2005**, *579*, 4851–4855.
28. Rao, R. K.; Basuroy, S.; Rao, V. U.; Karnaky, K. J.; Gupta, A. Tyrosine Phosphorylation and Dissociation of Occludin–ZO-1 and E-Cadherin–*b*-Catenin Complexes from the Cytoskeleton by Oxidative Stress. *Biochem. J.* **2002**, *368*, 471–481.
29. Zhang, X.; Sun, M.; Zheng, A.; Cao, D.; Bi, Y.; Sun, J. Preparation and Characterization of Insulin-Loaded Bioadhesive PLGA Nanoparticles for Oral Administration. *Eur. J. Pharm. Sci.* **2012**, *45*, 632–638.
30. Chen, M. C.; Sonaje, K.; Chen, K. J.; Sung, H. W. A Review of the Prospects for Polymeric Nanoparticle Platforms in Oral Insulin Delivery. *Biomaterials* **2011**, *32*, 9826–9838.
31. Teijeiro-Osorio, D.; Remunan-Lopez, C.; Alonso, M. J. New Generation of Hybrid Poly/Oligosaccharide Nanoparticles as Carriers for the Nasal Delivery of Macromolecules. *Biomacromolecules* **2009**, *10*, 243–249.
32. Nanosys, Inc. Systems and Methods for Nanowire Growth. U.S. Patent 20090124034, 2009.
33. Fogh, J.; Fogh, J. M.; Orfeo, T. One Hundred and Twenty Seven Cultured Human Tumor Cell Lines Producing Tumors in Nude Mice. *J. Nat.l Cancer Inst.* **1977**, *59*, 221–226.
34. Hidalgo, I. J.; Raub, T. J.; Borchardt, R. T. Characterization of the Human Colon Carcinoma Cell Line (Caco-2) as a Model System for Intestinal Epithelial Permeability. *Gastroenterology* **1989**, *96*, 736–749.
35. Yu, D.; Marchiando, A. M.; Weber, C. R.; Raleigh, D. R.; Wang, Y.; Shen, L.; Turner, J. L. MLCK-Dependent Exchange and Actin Binding Region-Dependent Anchoring of ZO-1 Regulate Tight Junction Barrier Function. *Proc. Natl. Acad. Sci. U.S.A.* **2010**, *107*, 8237–8241.
36. Bimbo, L. M.; Makila, E.; Laaksonen, T.; Lehto, V. P.; Salonen, J.; Hirvonen, J.; Santos, H. A. Drug Permeation across Intestinal Epithelial Cells using Porous Silicon Nanoparticles. *Biomaterials* **2011**, *32*, 2625–2633.
37. Neumeyer, A.; Bukowski, M.; Veith, M.; Lehr, C. M. Propidium Iodide Labeling of Nanoparticles as a Novel Tool for the Quantification of Cellular Binding and Uptake. *Nanomed. Nanotechnol.* **2011**, *7*, 410–419.
38. Balimane, P. V.; Chong, S. Cell Culture-Based Models For Intestinal Permeability: A Critique. *Drug Discovery Today* **2005**, *10*, 335–343.
39. Ingels, F. M.; Augustijns, P. F. Biological, Pharmaceutical, And Analytical Considerations with Respect to the Transport Media Used in the Absorption Screening System, Caco-2. *J. Pharm. Sci.* **2003**, *92*, 1545–1558.
40. Behrens, I.; Kissel, T. Do Cell Culture Conditions Influence the Carrier-Mediated Transport of Peptides in Caco-2 Cell Monolayers. *Eur. J. Pharm. Sci.* **2003**, *19*, 433–442.
41. Behrens, I.; Kamm, W.; Dantzig, A. H.; Kissel, T. Variation of Peptide Transporter (PepT1 and HPT1) Expression in Caco-2 Cells as a Function of Cell Origin. *J. Pharm. Sci.* **2004**, *93*, 1743–1754.
42. Artursson, P.; Karlsson, J. Correlation Between Oral Drug Absorption in Humans and Apparent Drug Permeability Coefficients in Human Intestinal Epithelial (Caco-2) Cells. *Biochem. Biophys. Res. Commun.* **1991**, *175*, 880–885.
43. Yasumatsu, H.; Tanabe, S. The Casein Peptide Asn-Pro-Trp-Asp-Gln Enforces the Intestinal Tight Junction Partly by Increasing Occludin Expression in Caco-2 Cells. *Br. J. Nutr.* **2010**, *104*, 951–956.
44. Alhamoruni, A.; Lee, A. C.; Wright, K. L.; Larvin, M.; O'Sullivan, S. E. Pharmacological Effects of Cannabinoids on the Caco-2 Cell Culture Model of Intestinal Permeability. *J. Pharmacol. Exp. Ther.* **2010**, *335*, 92–102.